ORIGINAL ARTICLE

lajss.org© Latin American Journal of Solids and Structures

www.lajss.org

Influence of filler material on the fragmentation characteristics of warheads

Cong Wang[a], Chenglong Wang[b], Fang Wang[a*], Tian Wang[a], Zhiwei Guo[a]

[a]State Key Laboratory of Explosion Science and Technology, Beijing Institute of Technology; Beijing 100081, P. R. China. Email: fang_w@bit.edu.cn, 3120210213@ bit.edu.cn, 3120220248@bit.edu.cn, Guozwbit@bit.edu.cn.
[b]Beijing Institute of Space Long March Vehicle, Beijing, P. R. China. Email: 350229858@qq.com.

*Corresponding author

https://doi.org/10.1590/1679-78258139

Abstract

A common issue with traditional warheads is the presence of a central blind zone when vertically striking targets. In this study, we proposed an axially reinforced warhead with different filler materials at the front end. Through experimental testing and simulations of single-point detonation at the bottom of the axially reinforced warhead, the fragmentation characteristics of the shell at the front end were analyzed, along with the fragment velocity and fragment distribution. The results showed that compared to traditional cylindrical warheads, the axially reinforced warhead filled with explosives or inert filler demonstrated significant improvements in fragmentation characteristics, the quality of the fragments, and the distribution of the fragments. Moreover, the fragment velocities showed greater similarity, and as the density of the inert filler increased, the improvement became more significant. In conclusion, the axially reinforced warhead with inert fillers at the front end produced evenly distributed fragments in the central damage area, which effectively improved the energy utilization of the warhead.

Keywords

Fragmentation characteristics; axially reinforced warhead; fragmentation; AUTODYN

Graphical Abstract

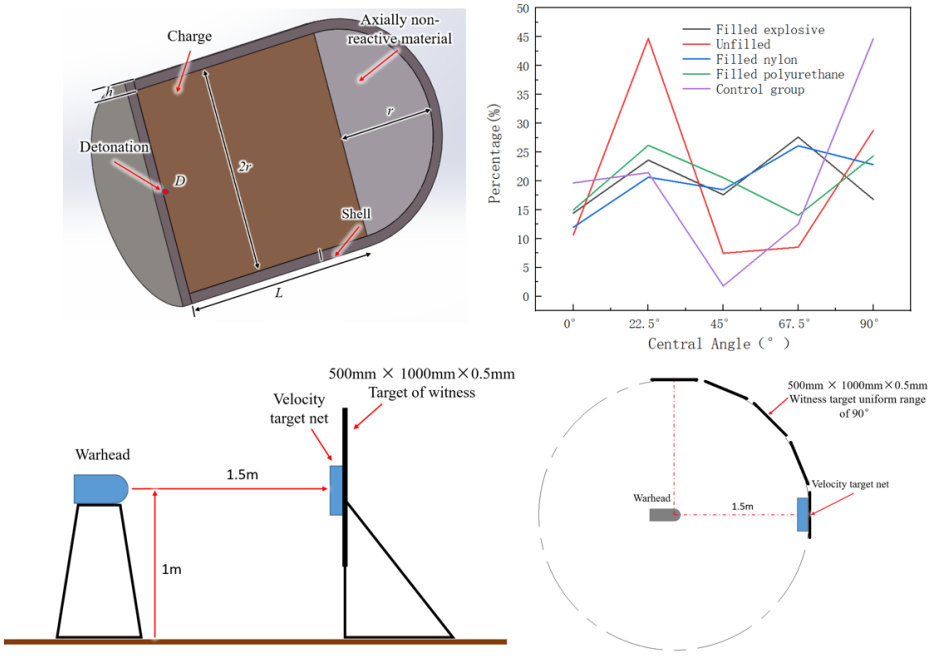

Received: April 02, 2024. In revised form: April 04, 2024. Accepted: April 09, 2024. Available online: April 11, 2024
https://doi.org/10.1590/1679-78258139

1 INTRODUCTION

Traditional fragment warheads typically use cylindrical explosives and set the detonation point on the rotational axis of the warhead to seek a higher destructive effect. However, when conventional warheads target an object directly in front, most of the fragments hit the surrounding area of the target, creating a large blind spot in the center of the target, resulting in incomplete damage. Currently, directional warhead technology has been able to enhance the radial fragmentation power of fragment warheads, but it has not addressed the issue of insufficient axial fragmentation and lack of effective killing power. Therefore, in order to solve the problem of the central blind spot in traditional fragment warheads when targeting vertically, Xie C B(2007), Dhote K D(2015), Ning J G(2017) introduced an axially enhanced fragment warhead. This type of axially enhanced warhead can create a larger range of fragment damage in the central area of the target, effectively causing damage to the target and filling the gap in the middle, as shown in Figure 1.

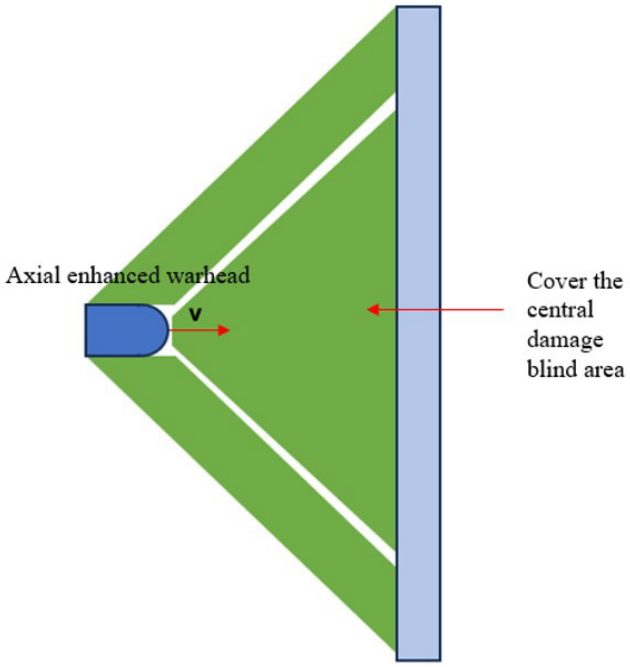

Figure 1 Fragment damage area distribution of Axial enhanced warhead

Zhao Yunchen et al(2016) studied the effects of the curvature radius of the warhead head shell, the thickness of the fragment layer, the thickness of the head shell, and the scattering characteristics of the forward-enhanced explosive fragments on the pre-positioned fragments. Tan Zhen et al(2018) explored the influence of the shape of the warhead head on the scattering characteristics of the axially enhanced prefabricated fragment warhead, and found that the arc-shaped warhead head has a better forward destructive effect than the flat plate-shaped warhead head, greatly increasing the power of axial destruction. Cui Junjie et al(2014) investigated the effects of the warhead head charge shape, fragment specifications, and arrangement on the initial velocity of the fragments scattered by the axially enhanced warhead. Xu Menglin et al(2022) explored the influence of the curvature radius of the spherical cavity, the length-to-diameter ratio of the charge, the shell thickness, etc., on the average scattering angle of the axially focused prefabricated fragment warhead with spherical cavity arrangement, and obtained the optimal combination.

This paper proposes a structure of an axially enhanced warhead with an inert material filled at the end, based on the differences in the propagation characteristics of the explosive shock wave in inert materials and in explosives. Through experimental verification and numerical simulation, the experimental and simulated values of the initial velocity and scattering angle of the fragments of the axially enhanced warhead under different inert filling materials are obtained, and the influence on their scattering characteristics is analyzed.

2 STRUCTURAL DESIGN OF THE AXIALLY REINFORCED WARHEAD

The structure of the axially reinforced warhead assessed in this study is shown in Figure 2, which was composed of two parts, namely, the main charge and the axial reinforcement. Specifically, the warhead contained high-energy explosives, a shell, and filler material at the front end. The warhead had a rotationally symmetric structure, where the

main charge consisted of a cylinder with a length of L = 40 mm and the axial reinforcement at the front end consisted of a hemispherical charge with a radius of r = 20 mm, which was tangent to the main charge. The warhead used natural fragments, where the shell thickness was h = 2 mm, and a B explosive was used. The detonation point was located in the center of the rear end of the main charge (point D), and the axial reinforcement was filled with various filler materials for comparison.

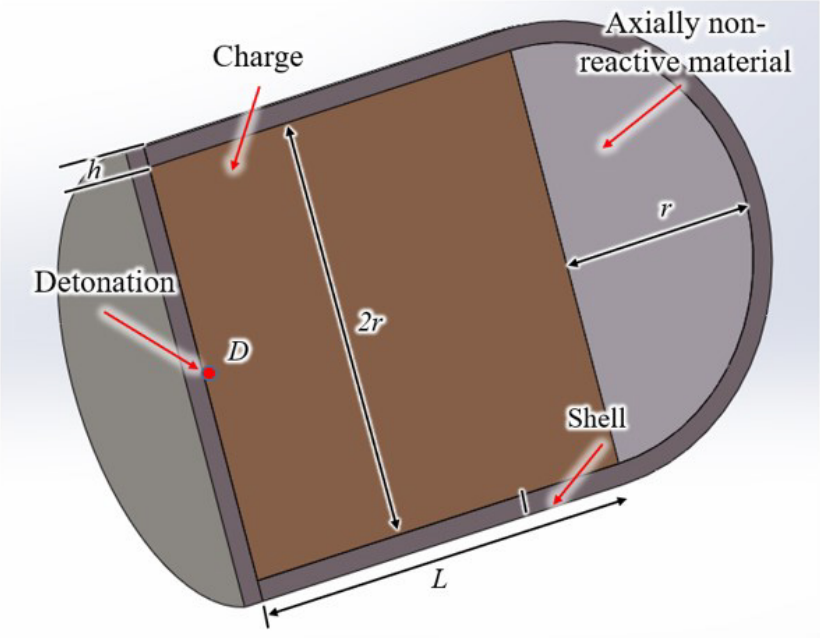

Figure 2 Detailed structure of the axial enhanced warhead

3 EXPERIMENTAL DESIGN

3.1 Specimens and basic principles

The warhead used in the experiments is shown in Figure 3, where the total length of the warhead was L = 60 mm, and the radius of the cylindrical portion and the radius of the hemispherical part at the front end were both r = 20 mm. The shell had a thickness of 2 mm and comprised of #45 steel. The detonator was installed in the bottom center of the warhead.

Figure 3 Physical diagram of the axial enhanced warhead

The experiments were conducted to evaluate the spatial distribution and velocity distribution of the natural fragments, and to analyze the axial reinforcement effects of different inert filler materials. The data was also used to validate the accuracy of the numerical simulations.

3.2 Experimental setup

A schematic diagram of the experiment is shown in Figure 4. The height of the warhead from the ground was 1 m, and 5 witness targets (500 × 1000 × 0.5 mm) were placed 1.5 m away from the warhead, which were evenly distributed within 0°–90°, with the warhead as the center. Therefore, the five witness targets were located at 0°, 22.5°, 45°, 67.5°, and 90°. In addition, a velocity target net was placed on each witness target to measure the velocities of the fragments. The layout of the experimental site is shown in Figure 5.

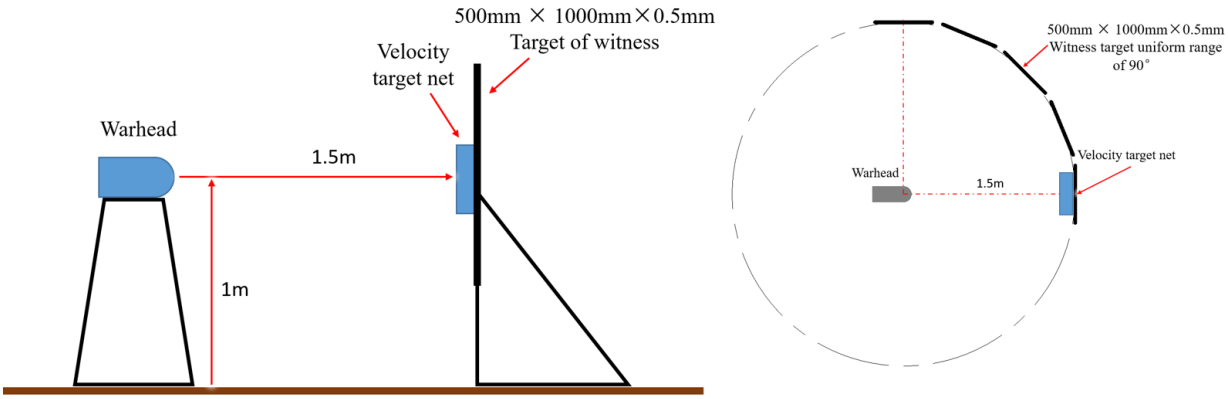

Figure 4 Schematic diagram showing the experimental layout

Figure 5 Layout of the experiment site

3.3 Experimental schemes

The experiments were divided into four groups according to the inert filler material. In group I, B explosive was used as the filler for axial reinforcement, while in group II, no filler was used. In Groups III and IV, nylon and polyurethane were used, and in Group V (the control group), the axial reinforcement part was removed, leaving only the cylindrical part. The total length of the warhead was 40 mm, with a radius of 20 mm and a shell thickness of 2 mm. The fragment velocity distribution and fragment quantity distribution in different regions were compared to evaluate the damage power of the warheads.

4 RESULTS

4.1 Fragment distribution in different regions

The perforations on the target plates in each group are shown in Figures 6−10.

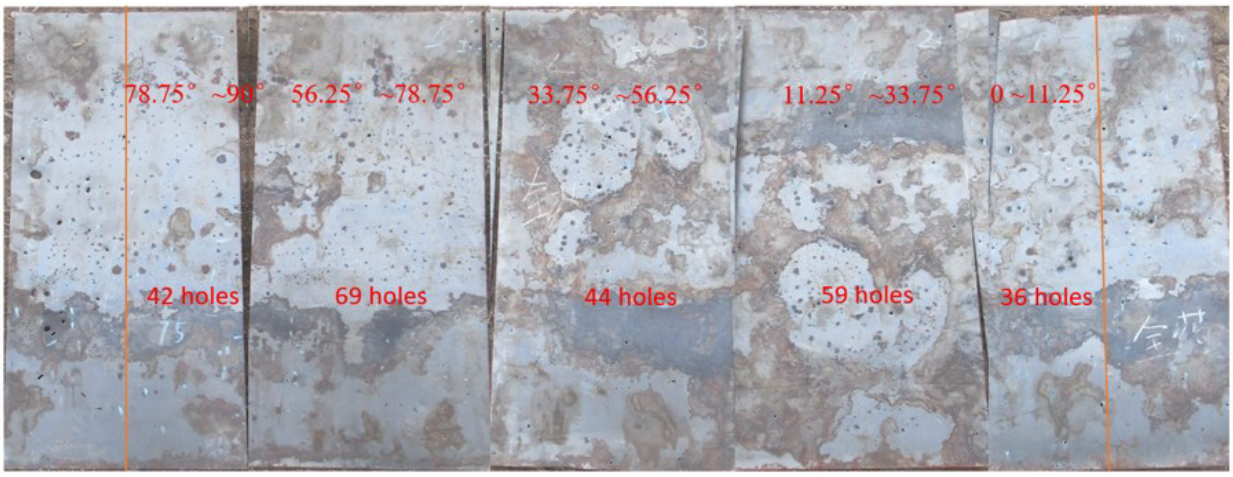

Figure 6 Perforation of the warhead filled with explosives

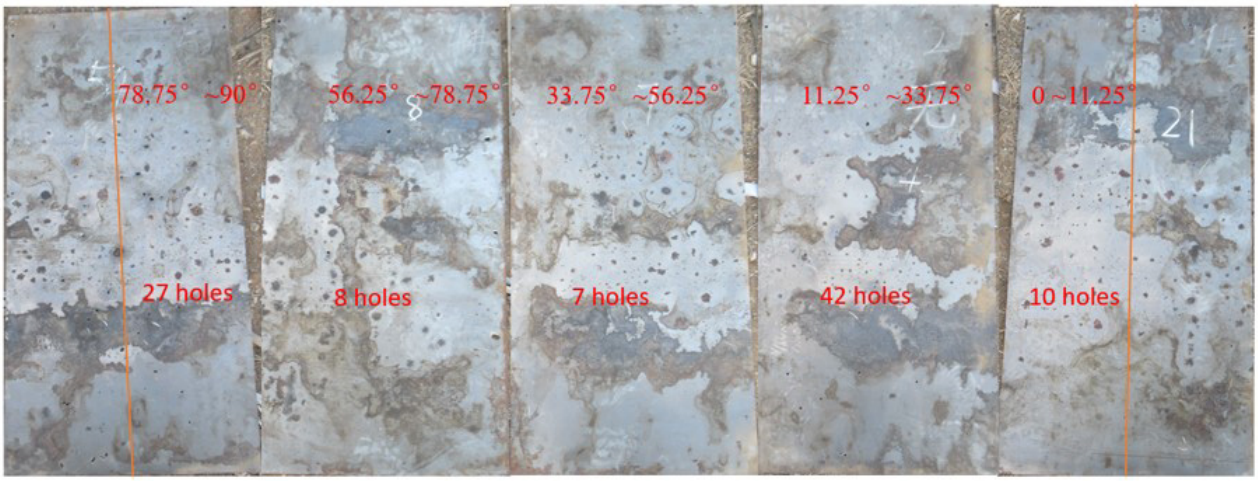

Figure 7 Perforation the warhead without filler material

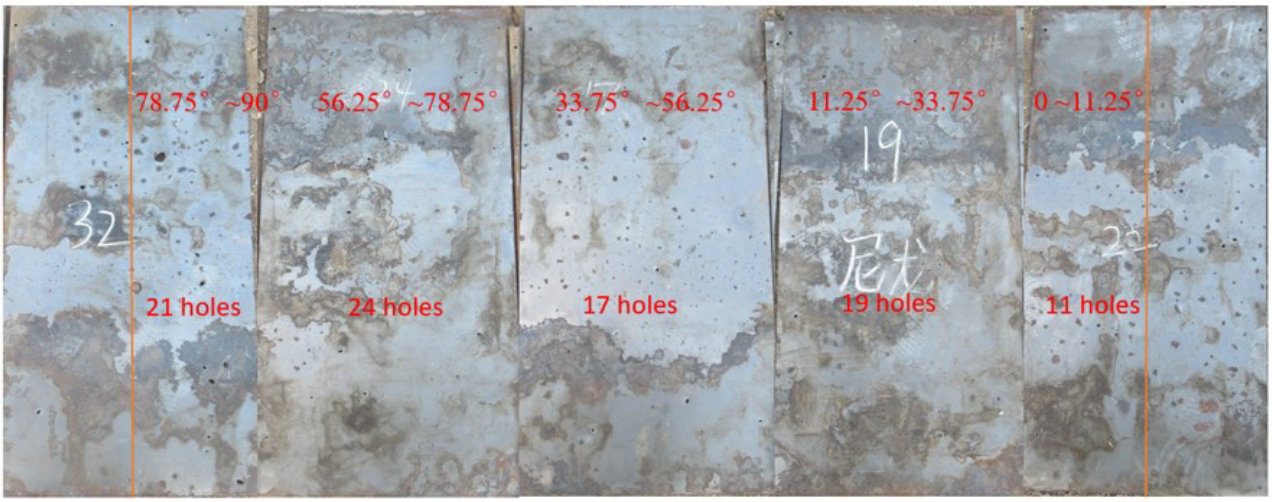

Figure 8 Perforation of the warhead filled with nylon

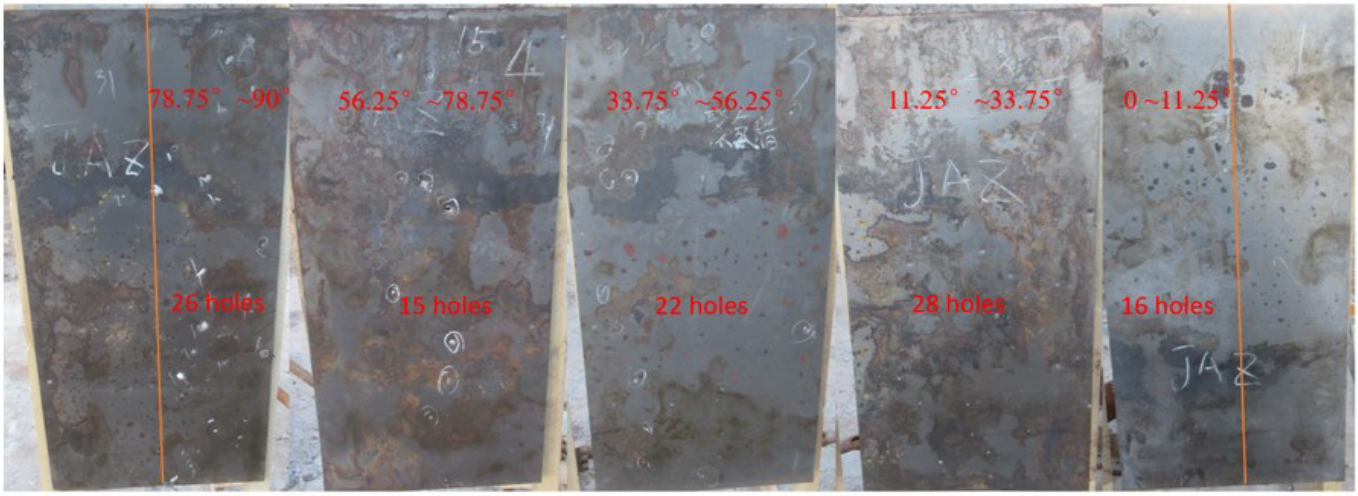

Figure 9 Perforation of the warhead filled with polyurethane

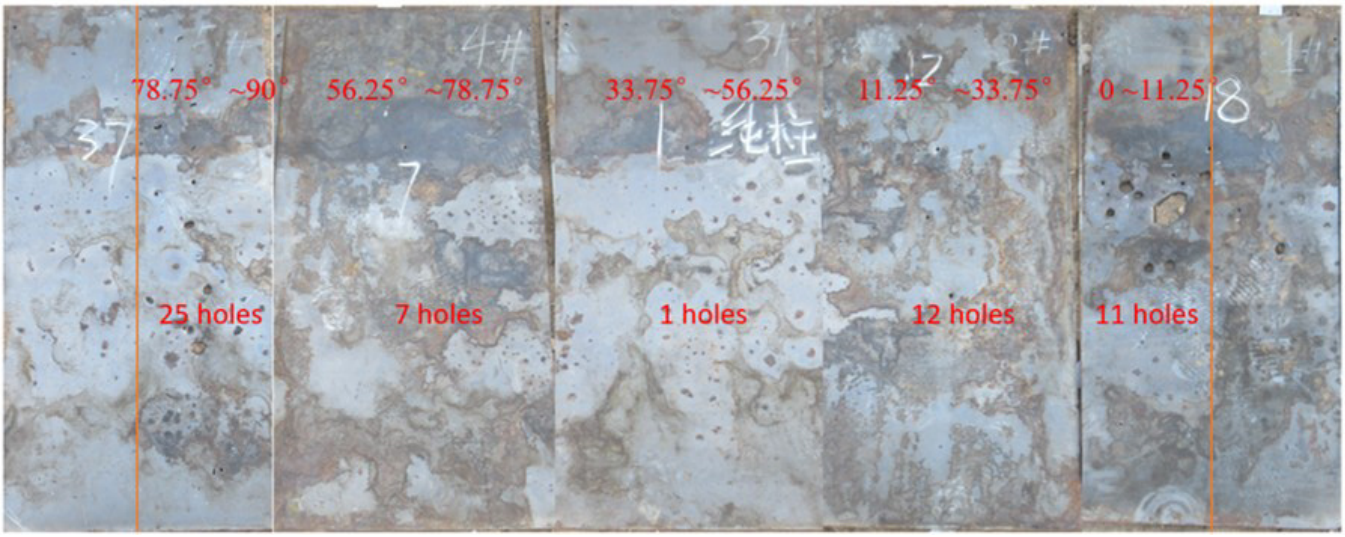

Figure 10 Perforation of the warhead in the control group

Because half of the target board at 0° and 90° is outside the range of 0° to 90°, when counting the number of target fragments statistically, the fragments outside the range need to be removed. In the end, the target board at 0° corresponds to a fragment distribution range of 0 to 11.25°, the target board at 22.5° corresponds to a fragment distribution range of 11.25° to 33.75°, the target board at 45° corresponds to a fragment distribution range of 33.75° to 56.25°, the target board at 67.5° corresponds to a fragment distribution range of 56.25° to 78.75°, and the target board at 90° corresponds to a fragment distribution range of 78.75° to 90°.

The number of fragments at each target plate in each group is shown in Table 1.

Table 1 Number of fragments captured by the target plates in each group

Angle to the center of the target plate	Warhead filled with explosives	Warhead without filler material	Warhead filled with nylon	Warhead filled with polyurethane	Control group
0°	36	10	11	16	11
22.5°	59	42	19	28	12
45°	44	7	17	22	1
67.5°	69	8	24	15	7
90°	42	27	21	26	25

We observed that group I contained the largest number of fragments, and the fragments were uniformly distributed among the target plates. This was because the large amount of explosive resulted in a significant degree of

fragmentation, forming small fragments. In groups II and V, the fragments were mainly concentrated at the two ends, with a limited number in the central area. In groups III and IV, the fragments were also most evenly distributed in different regions.

4.2 Fragment velocity distribution

The fragment velocity measured by the target net is shown in Table 2.

Table 2 Fragment velocity at different angles in each group

Angle to the center of the target plate	Warhead filled with explosives(m/s)	Warhead without filler material(m/s)	Warhead filled with nylon(m/s)	Warhead filled with polyurethane(m/s)	Control group(m/s)
0°	2405.77	4036.93	1760.20	2305.38	2411.71
22.5°	2448.97	3634.23	1486.91	1033.25	1691.13
45°	2243.82	/	1219.51	1896.33	/
67.5°	2064.69	1342.40	1506.99	1240.11	1759.60
90°	2177.06	1824.81	1854.21	1899.29	1722.71

Of note, the measured value of the velocity target net was the maximum velocity on the target plate. In groups II and V, no fragment was captured by the velocity target net on the 45° target plate, therefore, the fragment velocity was missing. According to the results, the fragment velocities measured at the 0° and 22.5° target plates in group II were very high, possibly because irregular fragmentation resulted in some small fragments, which had high velocities. In the 90° target plate, the velocity measurements were influenced by some fragments from the main charge, resulting in a high value.

5 NUMERICAL SIMULATIONS

5.1 Simulation model

The fragmentation behavior of warheads is often accompanied by large strain rates, large deformation, fractures, and fragmentation. Smoothed particle hydrodynamics (SPHs) is a meshless method that can minimize the impact of excessive mesh distortion on calculation accuracy. Additionally, because it is a pure Lagrangian method, it avoids the difficulty of capturing material interfaces using the Euler method. Hence, SPH can be used to simulate the fragmentation process of warheads and analyze the velocity distribution of fragments. Finite element simulation software AUTODYN was used to perform the numerical simulations in this study. The simulation models of the same dimensions were established based on the warhead dimensions in the above experiments.

An axially symmetrical 1/4 model was established (Figure 11) according to the rotational symmetry characteristics of the axially reinforced warhead. The main charge in the warhead was set as the B explosive, and the shell consisted of #45 steel. In addition, the material of the axial fragment shell was set separately to improve the readability of the axial fragment data. The particle radius was set to 0.4 mm in the SPH algorithm, according to a previous study of Li W (2015).

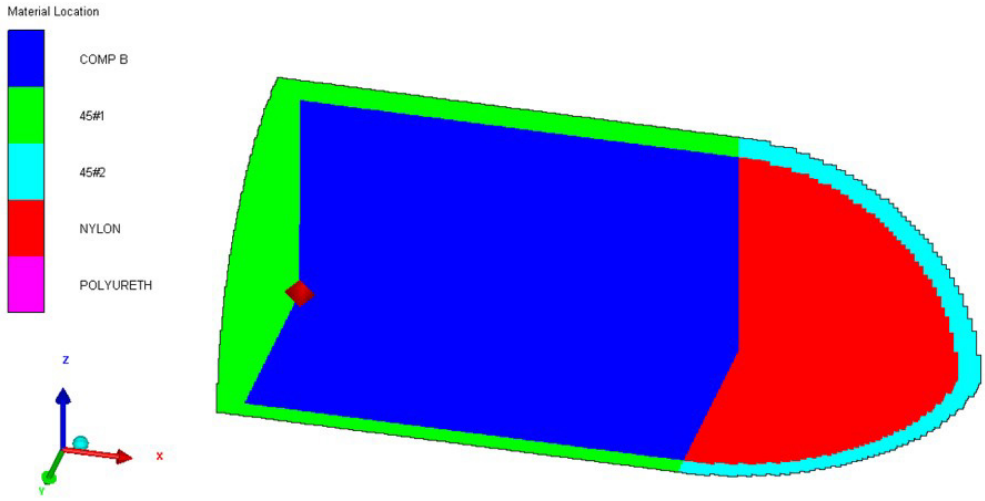

Figure 11 Simulation model of the axial enhanced warhead

5.2 Material properties

The shell consisted of #45 steel, which was described by the Johnson-Cook (JC) (1983) model:

$$\sigma = \left(A + B\varepsilon_{ep}^{n}\right)\left(1 + C\ln\dot{\varepsilon}^{*}\right)\left(1 - T^{*\mathrm{m}}\right) \tag{1}$$

where A is the yield strength, B denotes the strain strengthening coefficient, C is the strain rate strengthening coefficient, m and n denote the softening index and strain strengthening index, respectively, ε_{ep} represents the equivalent plastic strain,with being the plastic strain rate; $\dot{\varepsilon}_0 = 1.00s^{-1}$, which was the reference strain rate. In addition,T*=(T−Tr)/(Tm−Tr),where Tr is room temperature (293 K) and Tm is the melting temperature. In this study, the parameters of the JC model were obtained from Chen G, et al(2005). and the specific values are shown in Table 3.

Table 3 Material parameters of the #45 steel

Material	A (MPa)	B (MPa)	C	m	n	Tm (K)
AISI 1045	507	320	0.064	1.06	0.28	1793

The Jones-Wilkins-Lee (JWL) state equation(1985) was used for the B explosive:

$$p_e = C_1\left(1 - \frac{\omega}{R_1 V}\right)e^{-R_1 V} + C_2\left(1 - \frac{\omega}{R_2 V}\right)e^{-R_2 V} + \frac{\omega E}{V} \tag{2}$$

where p_e is the pressure of the detonation product, E denotes the internal energy volume, V is the initial relative volume, and C_1, C_2, R_1, R_2, and ω signify material parameters. The parameters of the JWL state equation for the B explosive were obtained from Dobratz B M.(1981) (Table 4).

Table 4 Material parameters and state equation parameters of the Comp. B

Material	Density *r* (kg/m³)	Detonation velocity *D* (m/s)	C-J pressure (GPa)	C_1 (GPa)	C_2 (GPa)	R_1	R_2	ω
Comp. B	1.717	7980	29	524	768	4.2	1.1	0.34

The dynamic response characteristics of the two types of inert filler materials (i.e., polyurethane and nylon) used in the axial reinforcement were described using the linear state equation and the shock state equation from Yun S R,et al. (1995). The Linear state equation is given by:

$$p = K\left(\frac{\rho}{\rho_0} - 1\right) \tag{3}$$

where K is the bulk modulus. The polyurethane parameters were obtained from Zhou, et al(2022) where the initial density was 300 kg/m³ and the bulk modulus was 37.3 MPa.

The Shock state equation for nylon is given by:

$$D = \mathrm{c}_0 + \lambda u_p \tag{4}$$

where D is the shock wave velocity, c0 denotes the sound velocity in the material, and λ is the coefficient of particle velocity up. The parameters were obtained from Matuska, et al(1975). where the initial density was 1140 kg/m³, the sound velocity was 2290 m/s, and λ =1.63.

5.3 Simulation results

Figures 12 to 16 present the simulated shell fragmentation process in each group, including the fragmentation condition at different time points and the distribution of the fragments.

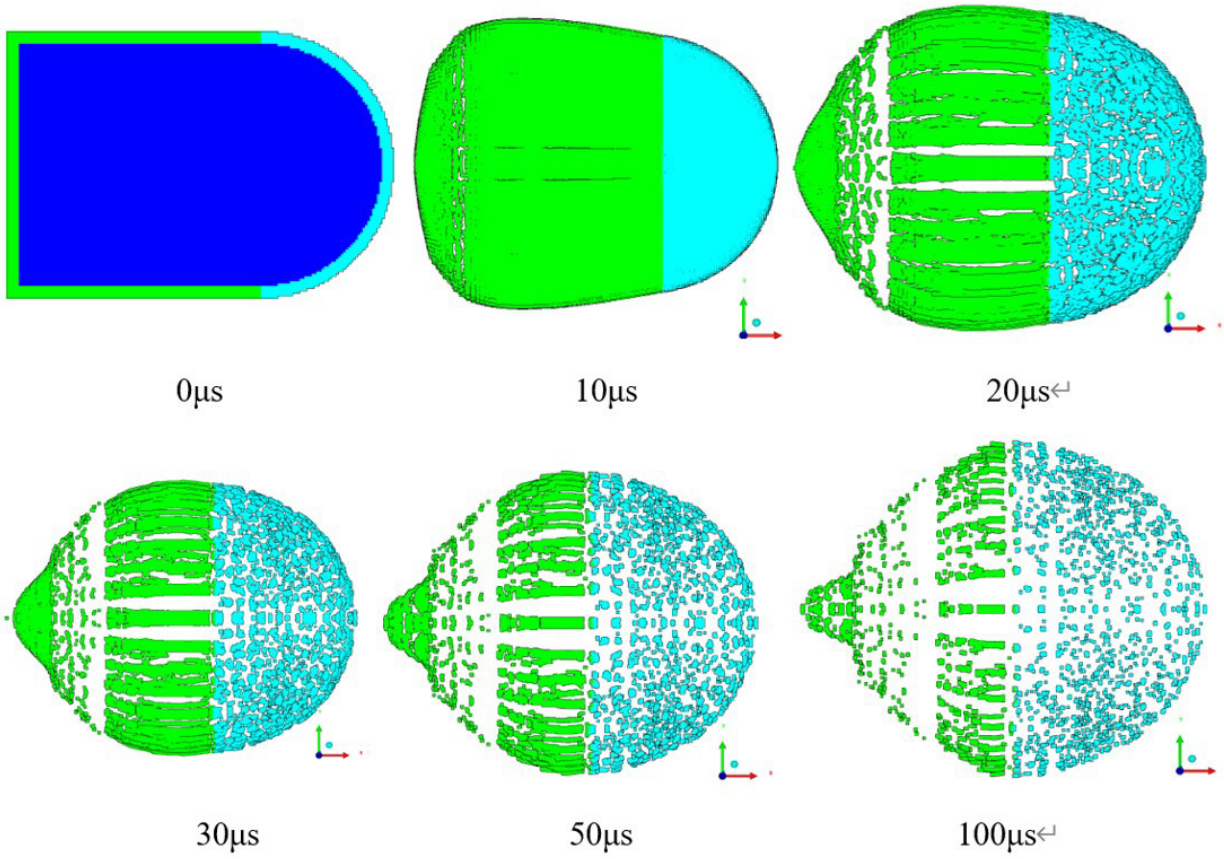

Figure 12 Fragmentation process of the warhead filled with explosives

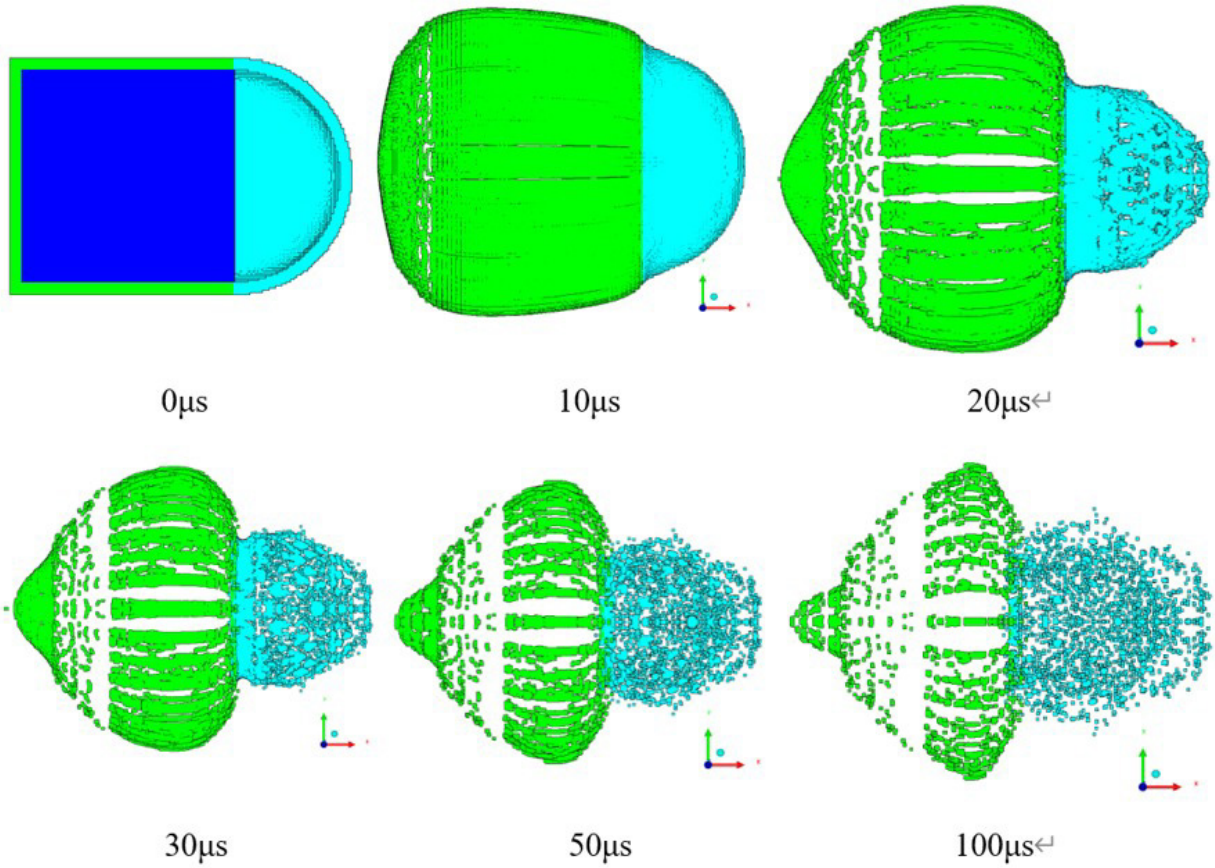

Figure 13 Fragmentation process of the warhead without filler material

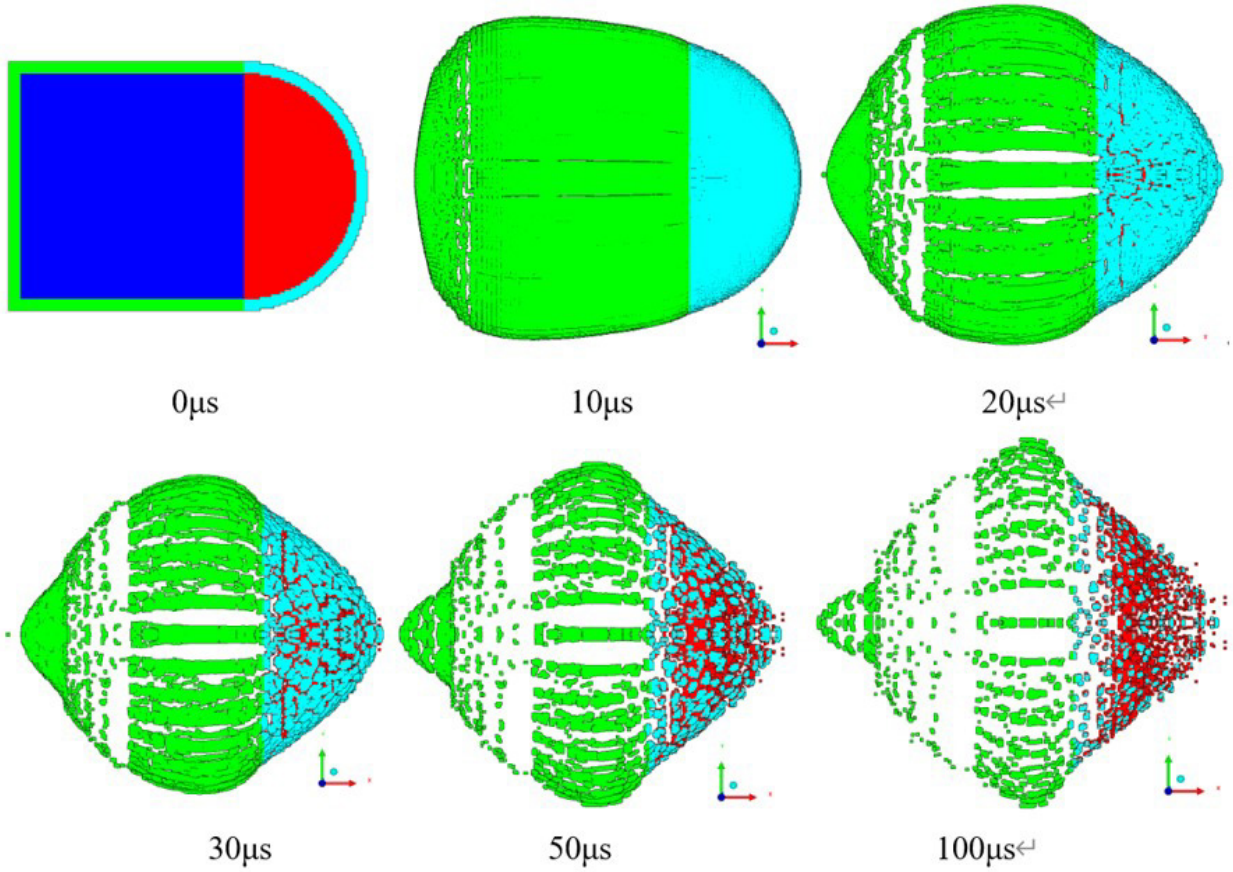

Figure 14 Fragmentation process of the warhead filled with nylon

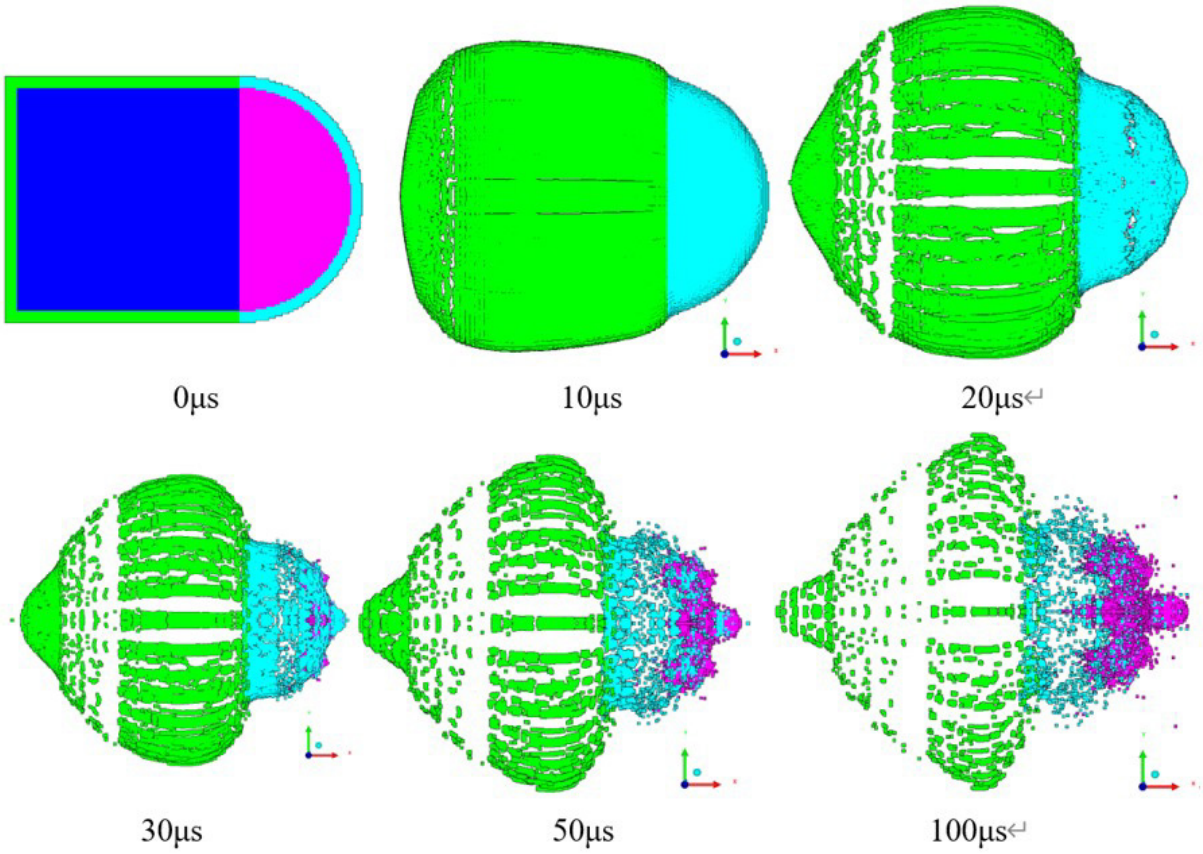

Figure 15 Fragmentation process of the warhead filled with polyurethane

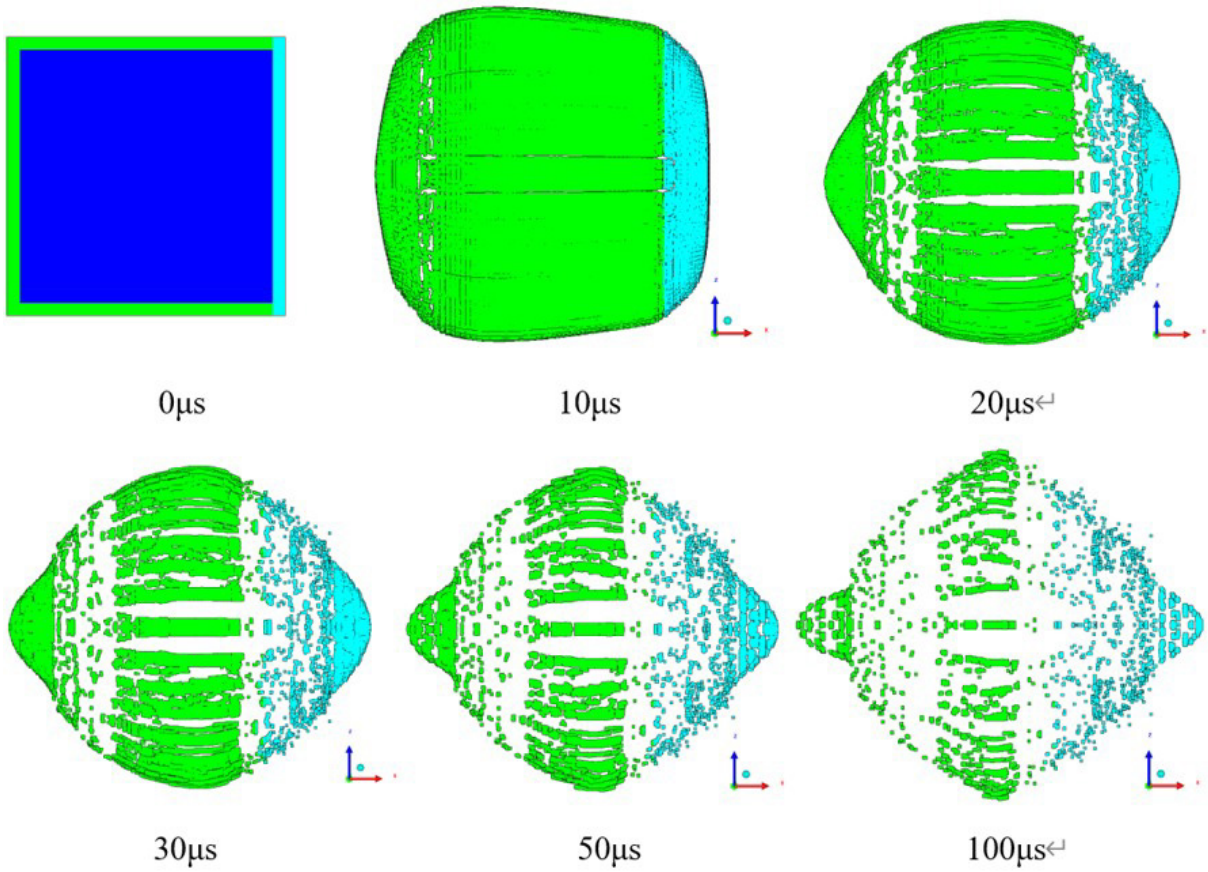

Figure 16 Fragmentation process of the warhead of the control group

According to the results, the fragmentation of the main charge was consistent between groups I–IV, suggesting that the filler materials did not have a significant influence on the main charge. In group V, the fragmentation was less ideal. Specifically, a large number of long fragments was found in the middle portion, with a small number of fragments on the target plate directly in front, which were concentrated in the center, indicating a poor damage effect on the target.

Explosive B was used in the axial reinforcement. The fragments were distributed evenly in a hemispherical shape, with a large number of fragments, and the mass of each fragment was small. This was because the detonation wave propagation increased the fragment velocity and caused a high degree of fragmentation.

When nylon was used as the filler material, the fragments were distributed in a cone shape, indicating inconsistent velocities of the fragments. Fragments closer to the central axis indicated a higher fragment velocity. Additionally, the degree of fragmentation was uniform. The mass of each fragment was larger than in group I, and the larger-mass fragments contained more severe damage than in group I. Moreover, the detonation wave from the main charge generated a strong shock wave in nylon, a reflecting shock wave or rarefaction wave formed back to the main charge, and the shock wave was absorbed and dissipated to a certain extent when it propagated in nylon. Consequently, the overall velocities of the fragments were reduced.

When polyurethane foam was used in the axial reinforcement, a clear boundary formed between the fragments of the front end and those from the main charge, and the fragments exhibited a spindle shape. This was due to the small density of the polyurethane foam, which resulted in significant shock wave absorption. Therefore, the intensity of the shock wave was lower than when nylon was used as the filler. As a result, the fragments near the main charge had low velocities and a low degree of fragmentation, while the fragments near the axis had high velocities and a high degree of fragmentation.

When no filler was used in the axial reinforcement, the fragments at the front end were distributed in an elliptical shape. This was because the fragments near the axis had high velocities, while the fragments far from the axis had low velocities and a low degree of fragmentation. Thus, the fragments were of varying sizes and masses.

According to the above results, the fragmentation characteristics of group II (i.e., no filler) showed the worst results. Among the inert filler materials, the fragments in group III demonstrated a better velocity distribution and mass distribution compared to in Group IV. In group I (B explosives), the fragment velocity increased due to additional charge, and the fragments were evenly distributed, resulting in a high degree of fragmentation. Therefore, the mass of the fragments was small, and the damaging effect on the target plate directly in front was inferior to that in the groups with inert filler materials.

6 COMPARISON BETWEEN THE EXPERIMENTAL AND SIMULATION RESULTS

6.1 Fragment distribution comparison

Based on the above experimental results, the percentage of fragments in each region was calculated for each group (Table 5, Figure 17).

Table 5 Percentage of fragments in each region

Angle to the center of the target plate	Warhead filled with explosives	Warhead without filler material	Warhead filled with nylon	Warhead filled with polyurethane	Control group
0°	14.4%	10.65%	11.95%	14.95%	19.65%
22.5°	23.6%	44.68%	20.65%	26.17%	21.43%
45°	17.6%%	7.44%	18.48%	20.56%	1.78%
67.5°	27.6%	8.51%	26.09%	14.02%	12.5%
90°	16.8%	28.72%	22.83%	24.30%	44.64%

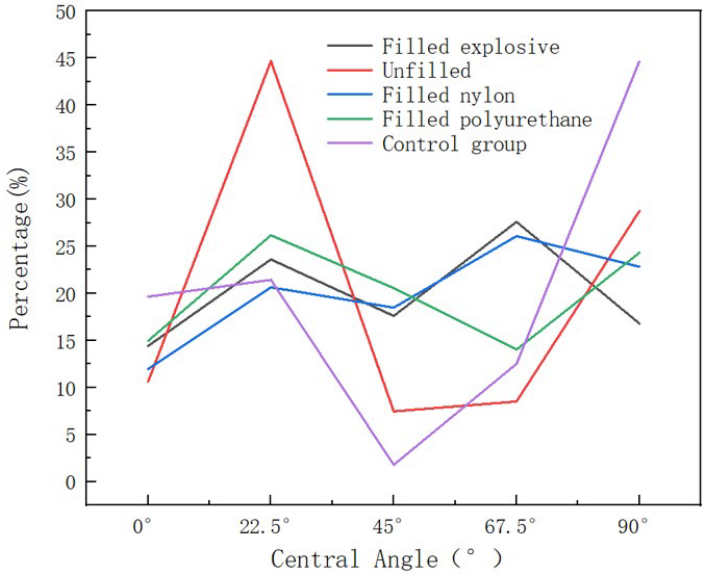

Figure 17 Distribution of fragments in each region.

We observed that the fragmentation results in groups II and V showed the worst results, with a large number of fragments located in the 0°−22.5° and 90° regions. In groups I, III, and IV, the number of fragments in each region was more uniform, improving the fragment utilization rate and avoiding the blind-zone problem found in traditional warheads.

The relationship between the flying angle and the azimuth angle for the fragments of different circumferential angles could be obtained for each group based on the simulation results. The fragment flying angles are shown in Figure 18, where the dotted line represents the outer normal azimuth angle of the axial reinforcement shell. The difference between the fragment movement direction and the outer normal direction of the shell was calculated from the distance between the numerically obtained fragment flying angle curve and the dotted line. Therefore, we could determine the extent to which the fragment flying angle was affected. In addition, as shown in Figure 18, regardless of the material used as the filler, the fragment movement direction angle was mostly below the dotted line. Therefore, the warhead fragments moved towards the front, and the difference between the fragment flying angle and the normal azimuth angle of the warhead shell increased with increasing azimuth angle. This was because single-point detonation at the center of the rear part of the main charge was used. As a result, when the detonation wave propagated to the axial reinforcement, the shell was subjected to an oblique forward-pointing force, thus, the flying angles of the fragments originated from different positions of the shell deviated in the axial direction to a certain extent.

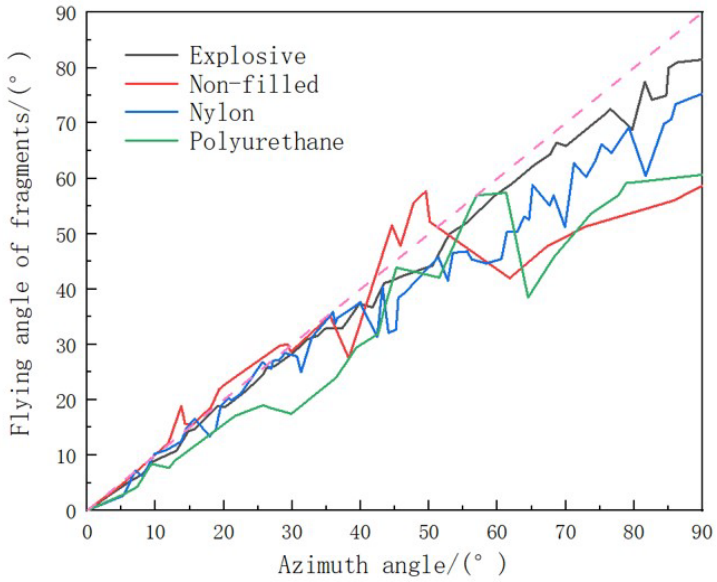

Figure 18 Fragment scattering angles of each group

According to the fragment scattering angle of each group, we observed that the curve of group II had large fluctuations, with one section of the curve above the dotted line. Therefore, the damage effect was poor. When polyurethane was used as the filler material, the curve was similar to that of group II, and the shell near the axis had a high degree of fragmentation. When the azimuth angle was greater than 60°, the scattering angle became stable and was significantly smaller than in groups I and III. Comparing groups I and III, we observed that the curves were basically the same when the azimuth angle was small. When the azimuth angle was greater than 60°, the fragment flying angle in group I was closer to the dotted line compared to group III. This was because the explosive contained a large amount of energy, increasing the radial acceleration of the fragments and causing an overall spherical shape. From groups III and IV, we observed that nylon with a larger density resulted in a more even fragment distribution.

6.2 Fragment velocity comparison

To further analyze the mechanism of filler material's impact on the fragmentation characteristics, the time history curve of the fragments at fixed positions was compared between the groups. The positions selected on the axial reinforcement are shown in Figure 19, the time history curves are shown in Figure 20, and the velocity values in each group are shown in Table 6.

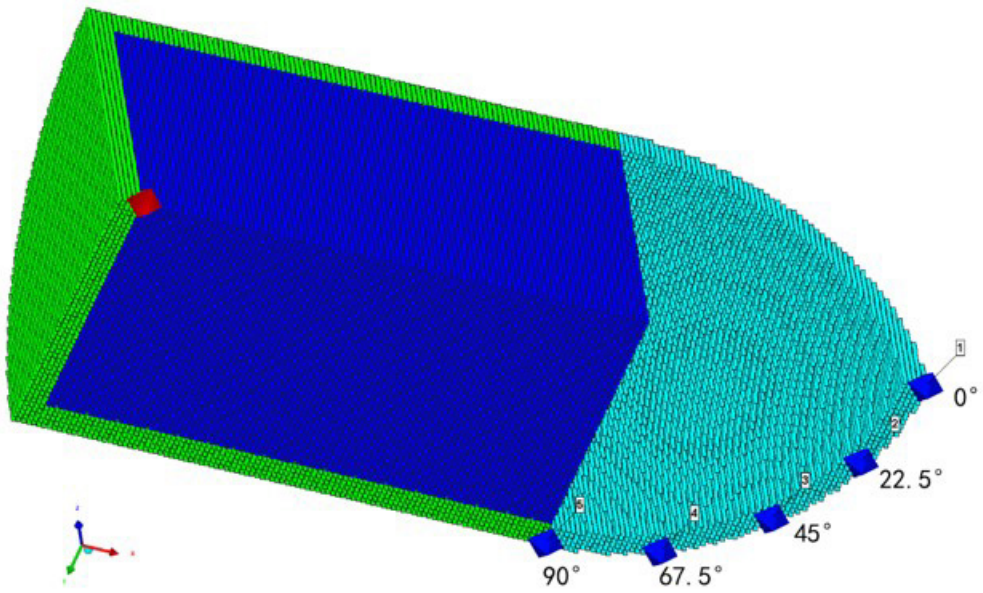

Figure 19 Schematic of Typical Fragment Position Selection in the Simulation Model

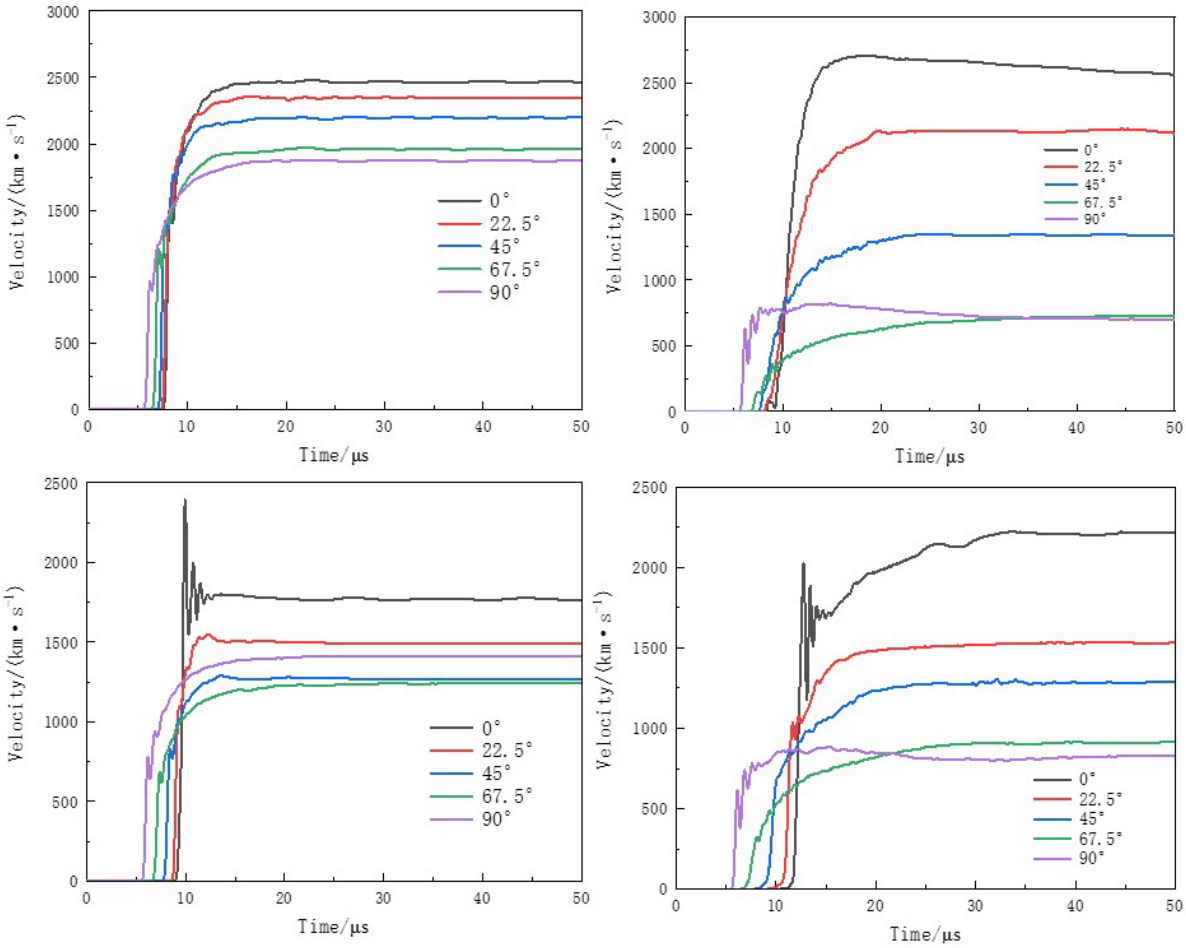

Figure 20 Typical positions selected for comparison

As shown in Figure 20,the first figure shows the velocity-time curve of groups I of simulated fragments, the second figure shows the velocity-time curve of groups II, the third figure shows the velocity-time curve of group III, and the fourth figure shows the velocity-time curve of group IV.

Table 6 Percentage of fragments in each region

Fragment circumferential angle	Warhead filled with explosives(m/s)	Warhead without filler material(m/s)	Warhead filled with nylon(m/s)	Warhead filled with polyurethane(m/s)
0°	2471.37	2560.87	1766.32	2220.18
22.5°	2349.56	2117.43	1487.78	1531.33
45°	2195.65	1341.89	1268.95	1286.23
67.5°	1958.34	726.026	1243.78	913.315
90°	1874.82	701.222	1412.84	826.633

Subsequently, the experimental and simulated fragment velocities in Tables 2 and 6 were compared. Because the fragment velocity measured in the 90° region during the experiment was affected by the fragmentation of the main charge, it was not included in the comparison. In addition, the experimental data for group II showed large variations, and therefore it was not included in the comparison. According to the results, the experimental and simulation results of groups I and III were very similar, with a difference of less than 10%. Because the experimental data showed the highest fragment velocity in an area, these values were expected to be slightly higher than the simulated values. In general, the simulation data was in good agreement with the experimental data of the two groups. For group IV, the difference between the experimental and simulated velocity was approximately 20%. This was likely due to the complex actions of the shock waves, which were difficult to simulate. However, the overall trend was basically consistent between the experimental and simulation results.

As shown in Figure 20 and Table 6, the fragment velocity became stable at 15 μs in groups I and III. Specifically, the fragment velocity in group I continuously and smoothly increased, because the additional charge significantly increased the acceleration time of the fragments. In comparison, the fragment velocity in group III changed with more fluctuations. This was consistent with the fact that the propagation velocity of shock waves in inert materials was lower than that of detonation waves. In groups II and IV, the fragment velocity stabilized after 20 to 30 μs, indicating the complex actions of detonation and shock waves.

Further, due to the additional charge in group I, the fragment velocity was higher than in the other groups, and the velocities of different fragments were similar, between 1900 and 2500 m/s. The fragment velocities in group III were concentrated (1300 to 1800 m/s), while the fragment velocities in groups II and IV were quite different, with a range of 700 to 2500 m/s and 800−2200 m/s, respectively. As a result, the damage effects were poor. In the initial stage, the fragment acceleration in groups I and III was significantly greater than in groups II and IV. The acceleration was the largest in group I, but showed rapid attenuation in group II. Therefore, we concluded that the use of inert filler material changed the release direction of explosion energy to a certain extent, which effectively increased the velocity of the lateral fragments and led to a more uniform energy distribution, i.e., fragment velocity, in all directions. Because the density of nylon was significantly higher than polyurethane foam, we concluded that as the density of the inert filler material increased, the impact on the energy release direction also increased.

7 CONCLUSION

To solve the blind zone problem of traditional warheads when vertically striking targets, in this work we proposed an axially reinforced warhead with different filler materials at the front end. Through experimental testing and simulations of single-point detonation, the fragmentation characteristics of the shell at the front end, as well as the fragment velocity and fragment distribution, were analyzed. The following conclusions were obtained.

(1) From the fragmentation characteristics, the traditional cylindrical warhead and warhead without filler materials exhibited the worst fragment shape and mass characteristics. In the group with explosive filler materials, the degree of fragmentation was the highest, the average fragment mass was the smallest, and the number of fragments was the largest. When inert filler materials were used, the force on the front end gradually became more even in all directions as the density of the filler material increased, resulting in better fragmentation characteristics.

(2) In the traditional cylindrical warhead and the warhead without filler materials, the fragments mainly flew perpendicular to the axial direction of the warhead. When explosive was used as the filler material, the fragments were evenly distributed throughout the area. When inert filler materials were used, the fragment distribution became more even throughout the area as the filler density increased, gradually approaching the fragmentation condition in the group filled with explosives.

(3) In terms of fragment velocities, the velocity decreased with increasing azimuth angle. The fragment velocities in the group without filler materials showed the fastest decrease, and the velocity difference between fragments was the largest. Additionally, a long period of time was required for velocity stabilization. When explosives were used as the filler material, the decrease in fragment velocity was the slowest, the velocity difference between fragments was the smallest, the fragment velocities were the highest overall, and the time required for velocity stabilization was the shortest. When inert filler materials were used, the decrease in fragment velocity became slower as the density of the inert filler increased, and the velocity distribution gradually became more uniform, thus, approaching the fragmentation condition in the group filled with explosives.

Author's Contribuitions: Conceptualization, Cong Wang and Zhiwei Guo; Methodology, Chenglong Wang; Investigation, Cong Wang and Tian Wang; Writing - original draft, Cong Wang; Writing - review & editing, Chenglong Wang and Fang Wang; Resources, Zhiwei Guo and Fang Wang; Supervision, Fang Wang.

Editor: Marcílio Alves

References

Xie C B. (2007) Simulation study on damage effect of axially Enhanced Warhead on air Target. Ph.D. Thesis, Nanjing University of Science and Technology.

Dhote K D, Murthy K P S, Rajan K M, et al. (2015) Directional warhead design methodology for a tailored fragment beam. Central European Journal of Energetic Materials 12(4): 637-649.

Ning J G, Duan Y, Xu X Z, et al. (2017) Velocity characteristics of fragments from prismatic casing under internal explosiveloading. International Journal of Impact Engineering 109: 29-38.

Zhao Y C. (2016) The study of fragment initial velocity and scattering direction of front fragment on forward enhanced lethal heprojectile. Nanjing, Jiangsu, China: Nanjing University of Science and Technology 15: 1-9.

TAN Z, Chen P W, Zhou Q, et al. (2018) Enhancement of axial lethality of warhead. Explosion and Shock Waves 38(4): 876-882.

Cui J J, Jiang J D, Niu X L, et al. (2014) The research on impacting factors of axial preformed fragment velocity. Journal of Projectiles, Rockets, Missiles and Guidance 34(2): 84-86;97.

Xu M L, Yin L K, Huang W L, et al. (2022) Axial preformed fragment focusing type Angle fragment warhead research. Journal of arrows of the guidance, 42 (4): 108-113.

Li W, Huang G Y, Feng S S. (2015) Effect of eccentric edge initiation on the fragment velocity distribution of a cylindrical casing filled with charge. International Journal of Impact Engineering 80: 107-115.

Johnson G R, Cook W H. (1983) A constitutive model and data for metals subjected to large strains, high strain rates and high temperatures. Proceedings of the 7th International Symposium on Ballistics. The Hague, Netherlands 12–21.

Chen G, Chen Z F, Tao J L, et al. (2005) Investigation and validation on plastic constitutive parameters of 45 steel. Explosion and Shock Waves 25(5): 69–74.

Dobratz B M, Crawford P C. (1985) LLNL explosives handbook, USA: Lawrence Livermore National Laboratory.

Dobratz B M. (1981) LLNL explosives handbook: properties of chemical explosives and explosives and explosive simulants. USA: Lawrence Livermore National Laboratory.

Yun S R, Tu H J, Jiang D S, et al. (1995) Explosion mechanics calculation method. Beijing, China: Beijing Institute of Technology Press.

Zhou Y, Wang T, Zhu W, Bia X, Huang G Y. (2022) Evaluation of blast mitigation effects of hollow cylindrical barriers based on water and foam. Composite Structures 282: 15-16.

Matuska D A, Needham C E, Durrett R E. (1975) Proceedings of the SIGNUM Meeting on Software for Partial Differential Equations. New York, USA: Association for Computing Machinery.